



**POLITECNICO**  
**MILANO 1863**

**SCUOLA DI INGEGNERIA INDUSTRIALE  
E DELL'INFORMAZIONE**

EXECUTIVE SUMMARY OF THE THESIS

# An AI-Enhanced Model of Athermal Fission Gas Release in SCIENTIX

LAUREA MAGISTRALE IN NUCLEAR ENGINEERING - INGEGNERIA NUCLEARE

**Author:** ARIANNA PAGANI

**Advisor:** PROF. DAVIDE PIZZOCR

**Co-advisors:** GIOVANNI ZULLO, LELIO LUZZI

**Academic year:** 2022-2023

## 1. Introduction

The investigation of nuclear fuel rod behavior under irradiation is fundamental for the safe design, licensing, and operation of nuclear reactors, as well as for studies on final repositories. One such crucial aspect is the behaviour of fission gas, particularly Xenon and Krypton. Fission gases precipitate into bubbles, causing fuel swelling and promoting pellet-cladding mechanical interaction. Additionally, fission gas release to the rod's free volume results in pressure buildup and thermal conductivity degradation. Various mechanisms of fission gas release exist, however, in this study the focus will be centered around athermal fission gas behaviour.

Athermal fission gas release holds prime importance in reactors that operate at low temperatures and, also, for fast neutron reactors using fuels with high thermal conductivity. Various mechanisms of athermal fission gas release exist. This study focuses on the athermal FGR induced by the presence of open channels in the fuel matrix. The as-fabricated porosity ( $P_{fab}$ ) contributes to a system of open tunnels of porosity at the grain edges, providing an easy escape path for gas atoms produced within the fuel grains. This system of percolated networks framing the grain is referred to as open poros-

ity ( $P_{op}$ ). While a prior model, developed by Claisse and Van Uffelen [1], accounting for the impact of open porosity on inter-granular fission gas release, is available in the open literature, it is believed to overestimate the release of fission gas due to oversimplifying assumptions. This investigation seeks to expand upon this model by incorporating physics-based approaches and machine-learning techniques.

The advancements resulting from the present work are incorporated into the SCIENTIX code [2] to enhance its predictive capabilities. Testing against literature data and benchmark scenarios, particularly in base irradiation cases, confirms the model's consistency and accuracy.

## 2. Methodology

### 2.1. Model development

The athermal fission gas release can be regarded as a venting process. This involves the release of gas by subtracting a portion of the gas concentration at grain boundaries, indicated as  $q$  (at  $m^{-3}$ ), resulting from diffusion and governed by Equation 1. This specific fraction is defined as the athermal venting factor ( $f_{ath}$ ).

$$\frac{\partial q}{\partial t} = (1 - f_{ath}) \left( D \frac{\partial c}{\partial r} \Big|_{r=a} \right) - R \quad (1)$$

where:  $D$  ( $\text{m}^2\text{s}^{-1}$ ) is the single-atom diffusivity,  $a$  (m) is the spherical grain radius,  $c$  (at  $\text{m}^{-3}$ ) is single-atom gas concentration and  $R$  (at  $\text{m}^{-3}\text{s}^{-1}$ ) is the released rate.

The nature of  $f_{\text{ath}}$ , according to Claisse and Van Uffelen (2015), is purely geometrical and relies on the polyhedral structure of the fuel grains. In this investigation, a corrective factor  $\lambda_{\text{ath}}$  for  $f_{\text{ath}}$  is defined to account for the real shape of the gas flux within the grain, including its dependency on the grain-edge inclination angle. This factor represents the ratio between the average integral flux exiting from the grain within the radius of the open porosity tunnel ( $\langle\varphi^{\text{out}}\rangle_{\text{op}}$ ) and the total average integral exiting flux ( $\langle\varphi^{\text{out}}\rangle_{\text{tot}}$ ).

$$\lambda_{\text{ath}} := \frac{\langle\varphi^{\text{out}}\rangle_{\text{op}}}{\langle\varphi^{\text{out}}\rangle_{\text{tot}}} \quad (2)$$

where:

$$\begin{cases} \langle\varphi^{\text{out}}\rangle_{\text{op}} = -\frac{2}{r} \int_r D \nabla c(x, y, t) dx dy \\ \langle\varphi^{\text{out}}\rangle_{\text{tot}} = -\frac{1}{l} \int_l D \nabla c(x, y, t) dx dy \end{cases} \quad (3)$$

Here, the specific value of  $r$  depends from  $P_{\text{op}}$ , which, in turn, a function of  $P_{\text{fab}}$ . To achieve a more physical interpretation of the relationship between  $P_{\text{op}}$  and  $P_{\text{fab}}$  the linear interpolation inferred by Claisse and Van Uffelen (2015)[1] was replaced by a new semi-empirical fit of the shape:

$$P_{\text{op}} = \underbrace{\alpha P_{\text{fab}}}_{\text{Isotropic term}} + \underbrace{\frac{a}{1 + e^{-c(P_{\text{fab}} - b)}}}_{\text{Anisotropic term}} \quad (4)$$

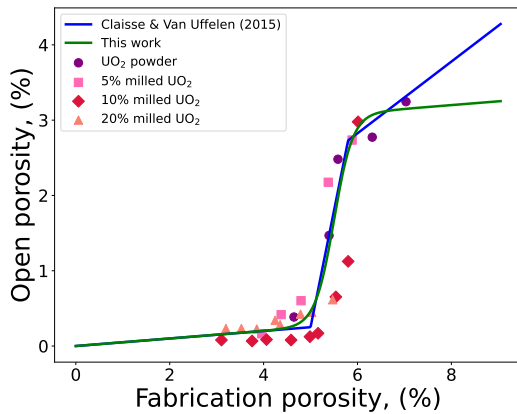


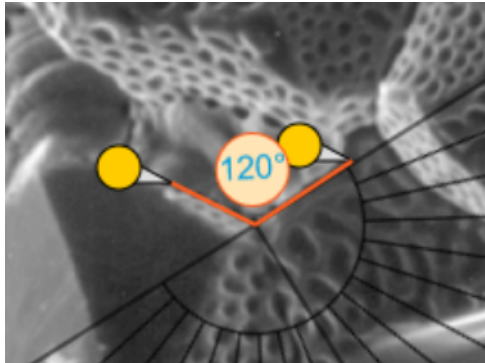
Figure 1: Comparison between this work's fit with the one inferred by Claisse and Van Uffelen [1]

With the scope of computing  $\lambda_{\text{ath}}$ , a numerical approach using finite element methods (FEM) is employed to solve the diffusion equation within a designated domain representing a 2-D section of the grain. Conducting a sensitivity analysis on the computed value of  $\lambda_{\text{ath}}$  in relation to the mesh coarseness revealed minimal variation. This suggests high fidelity of the computational method. Ultimately, the chosen value for mesh coarseness ensures accurate modeling of gas diffusion dynamics within the grain.

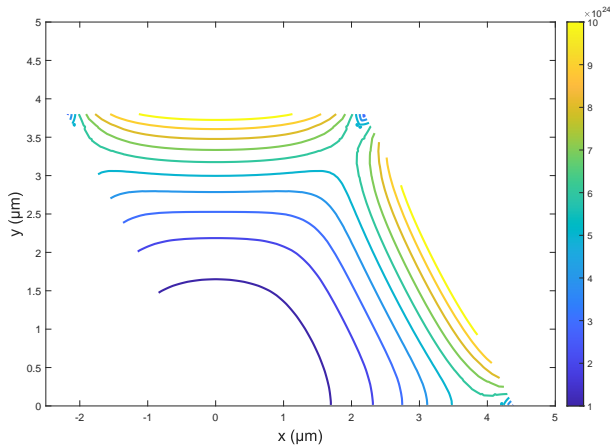
## 2.2. AI-enhanced model

In Section 2.1, we presented the fundamental physical conceptualization underlying our work. We introduced a corrective factor to the original formulation proposed by Claisse and Van Uffelen [1], accounting for the solution of the diffusion equation in a domain dependent on the grain-edge inclination angle. To compute this corrective factor, denoted as  $\lambda_{\text{ath}}$ , we utilized a high-fidelity (HF) MATLAB code to solve the diffusion equation, considering parameters such as grain-edge inclination angle ( $\theta$ ), fabrication porosity ( $P_{\text{fab}}$ ), grain edge length ( $l$ ), burn-up ( $\beta$ ), temperature ( $T$ ), gas generation rate ( $\dot{F}$ ) and gas initial concentration ( $C_0$ ). Of particular importance was the investigation of the grain-edge inclination angle  $\theta$  and its impact on gas diffusion. We inferred a validity range for  $\theta$  based on scanning electron microscope (SEM) images of nuclear fuel grains, spanning from approximately 90 to 135 degrees. By conducting simulations across various geometries, we observed how the gas diffusion gradient shape evolved with different values of  $\theta$  (Figure 2). As  $\theta$  increased, the concentration gradient within the grain became more uniform, eventually resembling the gradient in a spherical grain. The behavior of  $\lambda_{\text{ath}}$  was found to align with the trend of the concentration gradient, being small for  $\theta \approx 90$  and gradually increasing with higher values of  $\theta$ . Eventually, as  $\theta$  approached  $135^\circ$ ,  $\lambda_{\text{ath}}$  tended towards unity, indicating an alignment with Claisse and Van Uffelen's treatment of uniform gas diffusion. In addition to  $\theta$ , we discussed other factors influencing this phenomenon, including fabrication porosity, grain edge length, burn-up, temperature, and gas generation rate. These interdependencies highlighted the complexity of gas diffu-

sion within the fuel grain, necessitating a comprehensive approach in understanding and modeling its behavior.



(a)  $\theta = 120^\circ$ , SEM image from [3].



(b)  $\theta = 120^\circ$ ,  $\lambda_{\text{ath}} = 0.4573$ .

**Figure 2:** Evaluation of the gas diffusion gradient shape, accounting for the grain-edge inclination angle with the high-fidelity code.

Nonetheless, navigating these dependencies and their intricate physical interconnections posed complex challenges. Despite the precision achievable through the utilization of the HF code, the computational cost associated with its implementation proved to be burdensome and impractical for FPC applications. For these reasons, it was decided to encompass all the information relating to the aforementioned dependencies, feeding into the computation of the factor  $\lambda_{\text{ath}}$ , into a surrogate model. For the sake of explainability, a feed-forward neural network (FNN) was developed and integrated via a dedicated routine in the SCIANTIX code. The FNN was constructed featuring ten neurons and trained using synthetic data generated from the HF simulations, incorporating the various dependencies as input features. Furthermore, we

defined the validity ranges for each feature included in the surrogate model, ensuring that the model remains applicable within realistic operating conditions. The dataset was partitioned into training (70%), validation (15%), and test (15%) data according to a random sampling. The network’s training was optimized using the Levenberg–Marquardt algorithm, and its performance, evaluated in terms of mean square error (MSE), demonstrated its efficacy in capturing the complex relationships within the data.

### 3. Connected Phenomena

Various other phenomena significantly influence fuel behavior in low-temperature applications and impact the evolution of open porosity. Among these phenomena are solid swelling and fuel densification, both of which are crucial to comprehensively understanding fuel behavior.

#### 3.1. Solid Swelling

Solid swelling, as defined by Olander [4], quantifies the fractional increase in solid volume concerning the initial volume of fresh fuel. This phenomenon primarily stems from the replacement of heavy metal atoms by fission-product (FP) atoms, with contributions from both fission gases and other solid fission products. Typically, fission gases like xenon and krypton form bubbles within the fuel, while most other fission products exist as solids. However, at very low temperatures ( $T < 1000^\circ\text{C}$ ), fission gases may lack mobility to form bubbles, thus contributing to swelling similar to other fission products. In contrast with Olander in this work, this contribution, driven by the presence of Xenon and Krypton in intragranular solution, was kept separate from the one induced by FPs.

#### 3.2. Densification

As irradiation progresses, it’s expected that the initial open porosity in fuel diminishes due to in-pile densification. This process, influenced by factors like temperature, burnup, and fission rate, reduces the total porosity and consequently the open porosity. Empirical expressions, such as the one proposed by Van Uffelen [5], have been used to characterize the fraction of original fabrication porosity that anneals out due to densification. However, these empirical approaches

lack a deep understanding of the underlying physics. To address this, a semi-empirical approach was proposed in this study. Dependency on grain radius was disregarded for simplicity, as its influence on densification is uncertain in normal grain-sized grains. Instead, the densification process was modeled as burnup-dependent, with a temperature-dependent source term according to the following Ordinary Differential Equation (ODE):

$$\frac{df_{\text{dens}}}{d\beta} = k_{\beta} f_{\text{dens}} + S(T) \quad (5)$$

where  $k_{\beta}$  is a constants and  $S(T)$  is a source term, assumed exponential in nature. In this work, experimental data from a comprehensive study on  $\text{UO}_2$  fuel densification [6] were employed to tune the values of the constant  $k_{\beta}$  and refine the functional form of the source term. The densification factor is monotonically increasing with burnup to reflect the irreversible nature of densification. To account for residual porosity, a constant value of 75% of the initial fabrication porosity was assumed. Furthermore, the model addressed the densification of open porosity. Unlike previous assumptions, the fraction of original porosity and open porosity annealed out during irradiation were not assumed to be equal. Instead, Equation was enforced to dictate the new value of open porosity after densification. Overall, the proposed semi-empirical approach provides a comprehensive understanding of fuel densification, incorporating dependencies on burnup and temperature while considering the complexities of fabrication and open porosity evolution.

## 4. Results

The models developed in this work, integrated into the SCIANTIX code, were evaluated for consistency and predictive capabilities using open literature data. Separate effect tests were conducted to assess SCIANTIX's performance, employing Kashibe [7] and Baker [8] experimental cases as benchmarks. Furthermore, to expand the exploration of our AI-enhanced athermal fission gas release model, a synthetic dataset was generated. Covering the same fuel composition as the Baker tests, it spans temperatures from 373 to 2073 K and reaches a final burnup of 50 MWd/kg $\text{UO}_2$ . The test cases

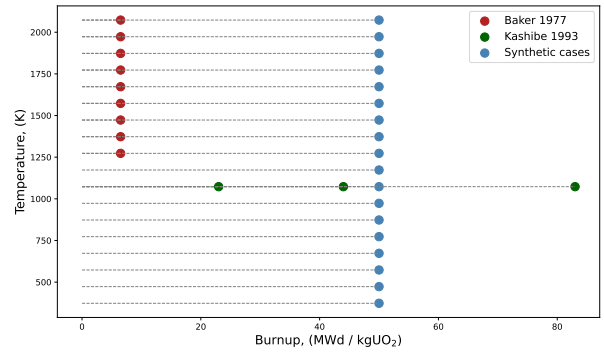


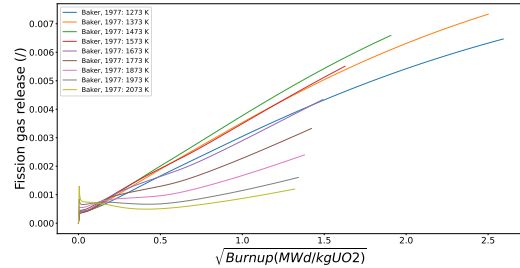
Figure 3: Experimental and synthetic cases employed in the separate effect tests of the AI-enhanced athermal fission gas release model developed in this work

are illustrated in Figure 3. Two reference cases were employed to effectively test the semi-empirical models for porosity densification and solid swelling. Namely, the Baker test case at 1273K and the Kashibe test base-irradiated under Pressurized Water Reactor (PWR) conditions were used with this scope. On one hand, this analysis underscored, in line with equation 4, the dual nature of the relationship between fabrication porosity and open porosity. Indeed, while the Baker case revealed the isotropic term of this linkage, the Kashibe one highlighted the anisotropic effect. On the other hand, the results of the solid swelling model noted how this quantity, during irradiation, closely follows the gas concentration in intragranular solution. The significance of integrating an athermal model into SCIANTIX was underscored through comparisons of fission gas release results, particularly with the model developed in [1] and with SCIANTIX without an athermal model. It was noted that the model developed in this study closely matched experimental observations of fission gas release across various scenarios, consistently maintaining levels well below 1%, except for the Kashibe case at 83 GWd/t. This deviation, however, was ascribed to the particular composition of the fuel employed in the test. Notably, variations were observed in the burnup values at which saturation occurs among the three models. The model without athermal release reached saturation first, followed by our prediction, and then by the Claisse model. This discrepancy in predicted burnup values for the onset of grain boundary saturation is note-

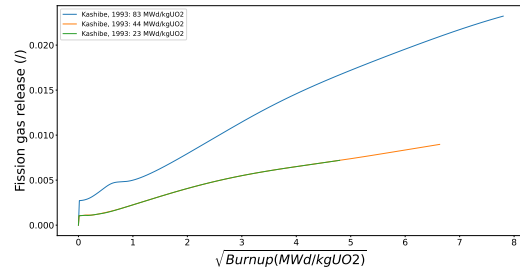
worthy. Although SCIENTIX operates as a 0-D code at a local level, this effect may carry importance for assessing regions within the fuel pellet where grain boundaries reach saturation. Having assessed the potential of the athermal fission gas release model developed within our research, our focus shifted towards examining its behavior across a wider spectrum of separate effect test cases, encompassing the Baker and Kashibe cases alongside a collection of synthetic cases, as mentioned before. To ensure clarity in our presentation, we truncated results concerning fission gas release histories upon reaching saturation. This approach facilitated a focused examination of athermal fission gas release, given that thermal diffusion dominates once saturation is achieved. Our findings were expressed in terms of a unique unit: the square root of burnup, aligning with the nature of FGR diffusion described by the Boot model. This metric provided a suitable approximation for short timescales, particularly relevant to low irradiation scenarios.

In evaluating the performance of our model across varying temperatures and low burnup levels using the Baker test cases, distinct trends emerged. Notably, an inverse relationship between incubation time and temperature was observed, alongside non-linear behavior in intergranular fractional coverage. Unexpected effects of temperature on fission gas release were also noted, such as peaks around 1700-1800 K, attributed to the mixed behavior of intragranular bubbles. The impact of densification on fission gas release was evident, resulting in a peak before the incipit of densification. However, the intertwining effects of temperature on densification and fission gas release hindered the establishment of temperature-bounds for this peak. Moving on to the Kashibe test cases, we explored our model's performance in low-temperature scenarios across extended burnup levels. Similar to the Baker cases, predominantly linear trajectories of fission gas release were observed, indicative of a primarily diffusive phenomenon. However, as burnup increased, this trend gradually diminished, particularly evident in the PWR test case. This was attributed to the short irradiation time approximation becoming invalid, as diffusion alone cannot fully explain the behavior of fission gas. Ad-

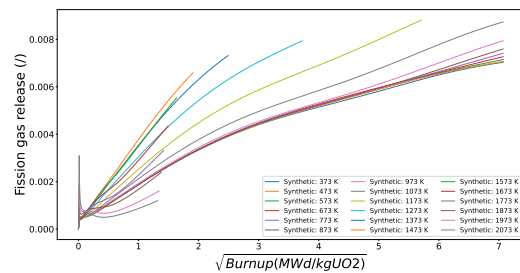
ditionally, the observations from these synthetic simulations mirrored those from the Baker and Kashibe cases, emphasizing the consistency of our model across the entire range of exploration. The results are reported in Figure 4.



(a) Fission gas release across the Baker experimental dataset.



(b) Fission gas release across the Kashibe experimental dataset.



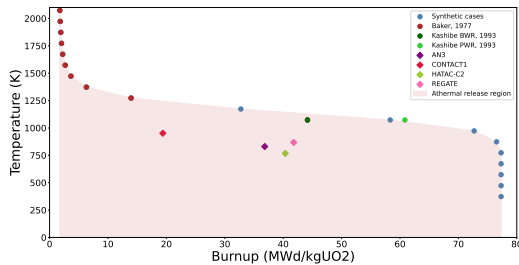
(c) Fission gas release across the synthetically generated dataset.

Figure 4: Athermal fission gas release, model evaluation across different separate effect test cases.

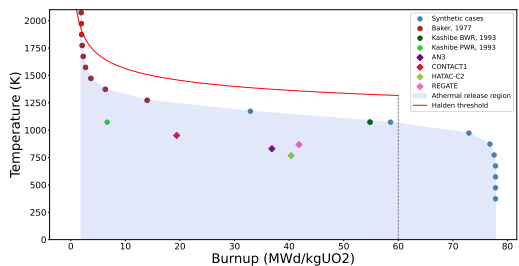
## 5. Discussion

Having studied in detail the behaviour of the AI-enhance model for athermal fission gas release developed in this study across a wide spectrum of temperatures and burnup levels, we turned our attention to the significance of our model for experimental cases utilized in validating the SCIENTIX code, including AN3, RE-

GATE, HATAC-C2, and CONTACT1. These experimental scenarios were evaluated at their respective average temperature. Results unveiled a compelling trend between the model's predictions and experimental observations, particularly in delineating the temperature and burnup levels at which saturation occurs. In our analysis of the temperature-burnup space mapping, distinct patterns were observed across various experimental cases. The Baker cases predominantly reside in a region characterized by low burnups and high temperatures, where saturation occurred rapidly upon irradiation onset. As temperatures increased, the incubation time exponentially decreased, followed by a slower linear trend observed in the Kashibe test cases. At higher burnup levels, this linearity diminished, indicating a threshold burnup value of approximately 77-78 MWd/kgUO<sub>2</sub> at which, across all temperatures, saturation is anticipated. Our model predicted that experimental points would predominantly lie in a region governed by athermal release, consistent with their observed fission gas release values.



(a) Mapping of the temperature-burnup space based on the coordinates at which fission gas release exceeds 1% for the different studied cases.



(b) Mapping of the temperature-burnup space based on the coordinates at which fission gas release exceeds 1% for the different studied cases, compared to the Halden threshold.

Figure 5: Fission gas release maps.

Furthermore, we constructed a similar map highlighting temperature and burnup values where fission gas release exceeds the 1% threshold. The Vitanza criterion - also known as the Halden threshold - was also incorporated for comparison and it consistently acted as an upper limit for the region of athermal release defined by our model. Once again, all experimental cases under consideration occupy a portion of the space governed by athermal fission gas release. Upon comparing the two maps (Figures 5), their similarity becomes evident. They describe the two-headed nature of fission gas release assessment. One pertains to the saturation of grain boundaries and dwells in the mesoscale. The other is centered on the engineering-oriented threshold of 1% fission gas release and inhabits the macro-scale. Thus, the convergence of these trends underscores the interplay between engineering and physical limits, revealing the intrinsic connection between the mesoscale and the macroscopic scale. All the experimental cases, consistent with their empirical data, were predicted to fall within the athermal release region, as delineated by both physics-based and engineering-oriented limits. As previously mentioned, these experimental data points were evaluated based on average temperatures. The SCIANTIX code operates at the mesoscale in a 0-D manner. Consequently, in the context of integral effect tests, it is not expected that the entire fuel rod will remain below the saturation limit. However, when considering a localized description of fuel behavior, the aforementioned observations remain relevant. Therefore, these maps can serve as a tool for assessing the predicted region of fission gas release, whether influenced primarily by athermal behavior or thermal diffusion. Ultimately analysis highlighted the relevance of an accurate model for athermal release, which is crucial for informing the design of experimental setups and fuel rods, as well as for the operation and licensing of nuclear reactors and final repositories.

## 6. Conclusions and Future Developments

This study investigated the significance of incorporating a model for athermal fission gas behavior in fuel performance applications. By focusing on the mechanism driven by open pore struc-

tures in the fuel matrix, we aimed to improve predictive capabilities using both physics-based models and machine learning techniques. We introduced a new quantity,  $\lambda_{\text{ath}}$ , to account for the real shape of gas flux exiting the fuel grain, considering factors like grain-edge inclination angle and diffusion dynamics. By incorporating a wide range of dependencies, a high-fidelity code provided accurate estimations of  $\lambda_{\text{ath}}$ , which were then used to train a feed-forward neural network for computational efficiency. In addition to the athermal release model, semi-empirical models for fuel solid fission products swelling and porosity densification were presented. Separate effect tests, including benchmark scenarios and synthetic cases, assessed the performance of the SCIANTIX code augmented by these models. Experimental data on fission gas release were further studied to explore the model's behavior, showing good agreement in base-irradiated scenarios. This study underscores the importance of developing a model for athermal release comprehensive of other relevant phenomena at low-temperature conditions, to inform both experimental setups and fuel rod design. Furthermore, the application of machine learning techniques in fuel performance codes offers significant potential for enhanced predictive capabilities without sacrificing computational efficiency. To advance this investigation, integral validation is crucial, along with efforts to enhance the explainability and interpretability of artificial intelligence techniques used. Additionally, uncertainty assessment and sensitivity analysis of introduced quantities would further improve the investigation's depth. Lastly, considering additional phenomena impacting on athermal fission gas release, could improve performance and accuracy.

## 7. Acknowledgements

- This work has received funding from the Euratom research and training programme 2021-2027 through the OperaHPC project under grant agreement no 101061453.
- This work has been partially supported by the ENEN2plus project (HORIZON-EUROATOM-2021-NRT-01-13 101061677) founded by the European Union.

## References

- [1] A. Claisse, P. Van Uffelen. Towards the inclusion of open fabrication porosity in a fission gas release model. *Journal of Nuclear Materials*, 466:351–356, 2015.
- [2] D. Pizzocri, T. Barani, L. Luzzi. SCIANTIX: A new open source multi-scale code for fission gas behaviour modelling designed for nuclear fuel performance codes. *Journal of Nuclear Materials*, 532:152042, 2000.
- [3] S. Valin, A. Mocellin, G. Eminent, S. Ravel. Modelling the behaviour of intergranular fission gas during out-of-pile annealing. Technical report, Cadarache, France, 9 2000. Fission Gas Behaviour In Water Reactor Fuels.
- [4] D.R. Olander. *Fundamental Aspects of Nuclear Reactor Fuel Elements*. Technical Information Centre, Office of Public Affairs Energy Research and Development Administration, Department of Nuclear Engineering University of California, Berkeley, USA, 1976.
- [5] P. Van Uffelen. *Contribution to the Modelling of Fission Gas Release in Light Water Reactor Fuel*. PhD thesis, Université de Liège, Liège, Belgium, 1 2002.
- [6] D. W. Brite, J. L. Daniel, N. C. Davis, M. D. Freshley, P. E. Hart. EEI/EPRI fuel densification project. Final report. UO<sub>2</sub>.
- [7] S. Kashibe, K. Une and K. Nogita. Formation and growth of intragranular fission gas bubbles in UO<sub>2</sub> fuels with burnup of 6-83 GWd/t. *Journal of Nuclear Materials*, 206:22–34, 1993.
- [8] C. Baker. The fission gas bubble distribution in uranium dioxide from high temperature irradiation SGHWR fuel pins. *Journal of Nuclear Materials*, 66:283–291, 1977).